Transportation Geotechnics 21 (2019) 100256

Contents lists available at ScienceDirect

Transportation Geotechnics

journal homepage: www.elsevier.com/locate/trgeo

A comparison of ground vibration due to ballasted and slab tracks

Evangelos Ntotsios[a,*], David J. Thompson[a], Mohammed F.M. Hussein[b]

[a] Institute of Sound and Vibration Research, University of Southampton, Southampton SO17 1BJ, UK
[b] Department of Civil and Architectural Engineering, Qatar University, Doha 2713, Qatar

ARTICLE INFO

Keywords:
Ground-borne vibration
Slab track
Ballasted track
Critical speed
MOTIV model

ABSTRACT

With the development of non-ballasted track forms (often referred to as slab tracks) over the few last decades, it is important to understand their behaviour with respect to ground-borne vibration compared with the traditional ballasted tracks. This is important in deciding between the use of the two track forms. The present work aims to quantify the differences between slab tracks and ballasted tracks numerically by using the MOTIV model. This is a general and fully coupled three-dimensional model that works in the wavenumber-frequency domain. It can predict the vibration levels of the track and the ground due to the gravitational loading of a passing train and the wheel and rail unevenness. A comparative analysis between the two track types is presented in terms of ground vibration with emphasis given to the influence of the stiffness and inertial parameters of the two track forms. It is shown that, for the same fastener stiffness there are only small differences in ground vibration behaviour, with the mass of the track slab leading to reductions of 1–3 dB at frequencies above 16 Hz. However, if softer rail fasteners are used in the slab track, as is usual, this leads to further reductions above 63 Hz. The critical velocity on soft soil is also considered. Although there is little difference between the different tracks for a homogeneous ground, for grounds with a soft surface layer the critical velocity is increased by the slab bending stiffness. The maximum rail displacement is also smaller for a slab track than the equivalent ballasted track.

Introduction

Railway track systems are under continuous development and many different structural forms have been introduced to fulfil different specifications. For over a hundred years conventional railway track was constructed with transverse sleepers laid on crushed stone (ballast). Initially sleepers were timber but from the 1930s onwards, as rolling stock speeds and axle loads increased, timber was gradually replaced by concrete and sometimes by steel. Through more than a hundred years of usage, the engineering knowledge of ballasted track has been refined, making it a highly-versatile and relatively low-cost track form. Nevertheless, the main weakness of ballasted track is the need for regular maintenance especially as the train speeds increase [1].

Driven mainly by the need to reduce maintenance costs, non-ballasted tracks were introduced from the 1960s and installed in tunnels and on bridges and viaducts. More recently, in order to accommodate the higher dynamic loading associated with high speed operation (for speeds greater than 200 km/h), non-ballasted tracks have been introduced in high-speed lines. Slab tracks are now increasingly being installed in different situations worldwide and, although they are more expensive to construct than ballasted track, they provide the desired long-term stability and rigidity for high speeds and good lateral and longitudinal resistance. A review of slab track systems with some further discussion of the design procedures and criteria, life-cycle costs, and implications for noise has been presented in [2].

In deciding between the use of ballasted or slab track there are many important technical and economic issues that have to be addressed. These primarily include construction cost, operability and environmental impact, mainly due to noise and ground-borne vibration. This work focuses only on the latter issue of the ground-borne vibration performance of ballasted and slab tracks for railways at grade.

Ground-borne vibration is generated at the wheel-rail contact and propagates through the ground to nearby buildings where it may cause nuisance for people or disturbance to sensitive equipment. Many different numerical models have been developed in the last decades that predict the vibration from surface and underground railways and which have been used to understand the generation and propagation of ground-borne vibration. A comprehensive overview of the state of the art on railway-induced ground vibration models and its excitation mechanisms can be found in [3]. The majority of these models are for ballasted tracks but there are also several that include slab tracks (e.g. [4–11]).

It has been shown that the track design affects the ground vibration for both surface and underground railway applications [4,12].

* Corresponding author.
E-mail address: e.ntotsios@soton.ac.uk (E. Ntotsios).

https://doi.org/10.1016/j.trgeo.2019.100256
Received 12 April 2019; Received in revised form 30 June 2019; Accepted 1 July 2019
Available online 16 July 2019

However, there are few comparative studies of the performance of slab track and ballasted track for ground vibration; most such comparisons have been made of the effect of the track design on the critical speed [13,14]. To the authors' knowledge, the only work in the literature that studies and compares track and free-field vibration levels due to train passages between ballasted and slab tracks is included in [15]. However, this work emphasizes comparisons with floating slab tracks. These provide an effective way to reduce vibration transmission from railway traffic to the ground by adding an elastic bearing beneath the slab [6–8]. Although these special track forms are very effective and widely used in modern underground lines, they are not the main focus of the current study.

The aim of this paper is to study numerically the comparative performance in terms of ground-borne vibration of slab tracks and ballasted tracks located at the ground surface. The MOTIV model, a semi-analytical three-dimensional model is used. This is a versatile and fully coupled model that is based on the formulations originally developed in [16] for surface railways and in [17,18] for tunnels. It is formulated in the wavenumber-frequency domain and uses transfer function matrices for the ground expressed in a moving frame of reference. Thus, it includes the effects of the moving loads and can also be used to assess the critical velocity. The model is presented in more detail in Section 'The MOTIV model'.

There are many different types of ballasted and slab tracks in use around the world. Thus, it would not be feasible to compare the ground vibration performance of every track type, including different rail types, fastening systems, sleeper or slab designs, and subgrade-improvement processes. Moreover, the ground-borne vibration performance is strongly related to the ground properties of a given railway site and also to the rolling stock that operates on the line. Experimental comparisons have many drawbacks due to inherent differences between the tracks that are compared, for example due to the soil conditions or the track unevenness. Thus, this work aims to identify only the main differences in predicted vibration levels between generic ballasted and slab track designs and to highlight the major characteristics that can affect these vibration levels. The description and properties of these generic tracks are based on [19] for the ballasted track and on the Rheda 2000 specifications [20] as a typical slab track. The assumed properties are given, together with the properties of the ground for a range of soil conditions, in Section 'Track-ground system properties'.

Section 'Loads applied directly on the ground surface - ground dispersion' presents a study of the dispersion characteristics and the wave propagation mechanism for the selected ground types. This forms a basis for providing a better insight into the track-ground interaction and the free-field vibration that are presented in Sections 'Ground dispersion for different track forms and the effect of load speed', 'Ground vibration due to train passages' and 'Critical speed for different track forms'. Using the MOTIV model a comparison is made first for vibration due to single dynamic loads in Section 'Ground dispersion for different track forms and the effect of load speed', and then due to train passages in Section 'Ground vibration due to train passages'. Finally, in Section 'Critical speed for different track forms' simulation results are presented to indicate the speed at which critical velocity effects occur for the different track forms.

The MOTIV model

The MOTIV (Modelling Of Train Induced Vibration) model [21] is a semi-analytical computational tool for calculating ground vibration from surface and underground railways and for assessing the performance of vibration countermeasures at the track and/or the train. The model has a graphical user-friendly interface and it uses state-of-the-art techniques to perform quick predictions of vibration levels in the vicinity of the track and in the far field. For ground vibration from surface railways, use is made of the formulation originally developed by Sheng et al. [16]. This has recently been extended in [22] to take into account the traction variation across the track-ground interface and to allow the excitation and response of the two rails to be considered separately. For underground railways, not considered here, the model uses the formulation developed in [17,18] that was later extended in [23] to include layered soil conditions.

For surface railways, studied here, a longitudinally invariant ballasted or slab track is coupled vertically to the surface of the ground. No coupling is made in the lateral direction at the soil surface. The track structure is modelled as multiple beams supported by vertical springs with consistent mass and the soil is modelled as a horizontally layered halfspace. Linear dynamic behaviour is assumed throughout. The excitation is assumed to be due to the passage of individual wheel loads along the track (quasi-static loading) and due to dynamic interaction forces caused by irregularities of the wheels and tracks (dynamic loading). The model is formulated in the wavenumber-frequency domain and uses the transfer function matrices for the ground formulated in [24] in a frame of reference moving with each load at speed v. Thus, it includes the effects of the moving loads and predicts the vibration level at a fixed point in the free field during the passage of the train.

Following the formulation presented in [22], the track (ballasted or slab) exerts a distributed load on the ground. This is applied by discretizing the interface conditions between the track and the ground. The discretization introduces a finite sum of the normal tractions at the track/ground interface: across the interface, there is a finite number of strips; within each strip, the stresses are assumed constant and displacement compatibility is required along the centrelines of the strips. This allows the rotation of the sleepers or the slab (and the wheelsets) about the axial direction to be included, excited by non-symmetrical unevenness of the two rails.

Only the vertical interaction forces are considered and only the vertical dynamics of the train are included. The train is modelled as a linear multiple rigid-body system and the flexible modes of the car body are neglected. This is generally acceptable for ground-borne vibration because the vehicle's suspension isolates the car body above about 10 Hz. Therefore, above 10 Hz, the vehicle's unsprung mass is the only component that affects the vertical dynamic loads. Below 10 Hz, it was shown in [22] that non-symmetric loading at the wheel/rail contact points is usually negligible, and therefore the rolling modes (rotation around x-axis) of the car body and the bogie are not excited. Thus, the car body and bogies can be further simplified as having only two degrees of freedom (DOFs), i.e., the vertical displacement of their mass centre and pitch motion (around y-axis). Similarly, each wheel has only one DOF, i.e. its vertical displacement. The coupling between vehicles is neglected and to enable analysis in the frequency domain each non-linear suspension is linearized, which is valid for small motion amplitudes. Hysteretic, viscous or viscoelastic damping can be included in the stiffness elements of the vehicle suspension.

The vehicle parameters that are used for all simulations within this study are listed in Table 1, see also Fig. 1. These are taken from [25] and correspond to a typical electric multiple unit (EMU) train. The primary and secondary suspensions are represented by visco-elastic elements, as shown in Fig. 1(b); their dynamic stiffnesses are given by $k_p = \frac{k_{p1}k_{p2} + i\omega c_p(k_{p1}+k_{p2})}{k_{p2} + i\omega c_p}$ and $k_s = \frac{k_{s1}k_{s2} + i\omega c_s(k_{s1}+k_{s2})}{k_{s2} + i\omega c_s}$ respectively.

It is assumed that the wheel is always in contact with the rail. A linearized Hertzian contact spring is included between each wheel and the rail, although for the frequency range of ground-borne vibration (below 250 Hz), inclusion of the contact spring does not influence the total response significantly. Moreover, the wheel irregularities are neglected, so that all irregularities are assumed to be on the rail surface and the vertical profile of the rail may be decomposed into a spectrum of discrete harmonic components. The relation between the angular frequency ω of the dynamic loading and the wavelength λ of the rail irregularity is $\omega = 2\pi v/\lambda$, where v is the velocity of the train.

The rail unevenness spectra that are used for all simulations within this study are shown in Fig. 2; the average unevenness spectra of the

Table 1
Assumed vehicle parameters.

Car body	Mass	m_c = 26, 200 kg
	Pitching moment of inertia	$J_c = 2{\cdot}10^6$ kg·m^2
	Overall vehicle length	l_v = 20 m
	Number of vehicles	N = 4
Bogie	Mass	m_b = 5000 kg
	Pitching moment of inertia	J_b = 6000 kg·m^2
	Half distance between bogie centres	l_b = 7.1 m
Wheelset	Mass	m_w = 1800 kg
	Total axle load	P = 106.5 kN
	Contact stiffness (per wheel)	k_H = 1.26 GN/m
	Half distance between axles	l_w = 1.3 m
Primary suspension	Vertical stiffness per axle	k_{p1} = 0.85 MN/m
	Vertical viscous damping per axle	c_p = 20 kN·s/m
	Series stiffness per axle	k_{p2} = 85 MN/m
	Spring lateral half distance	l_p = 0.9 m
Secondary suspension	Vertical stiffness per axle	k_{s1} = 0.6 MN/m
	Vertical viscous damping per axle	c_s = 20 kN·s/m
	Series stiffness per axle	k_{s2} = 60 MN/m

two rails are shown in one-third octave band form in Fig. 2(a) and the coherence functions between the left and right rail profiles for the wavelength range from 40 m to 0.5 m are shown in Fig. 2(b). These unevenness spectra have been obtained from measured data from two typical tracks in the UK, a ballasted track and a slab track reported in [22].

The unevenness spectrum for the ballasted track has been obtained using two measurement systems [26]. The short wavelength range was measured using a corrugation analysis trolley (CAT) [27]. Longer wavelength data (greater than 0.5 m) was obtained from routine measurements of vertical track alignment using a track recording coach (TRC), which yields loaded track profiles. For wavelengths longer than 35 m, where the accuracy of the TRC is not guaranteed, the spectrum has been extrapolated.

For the slab track, the unevenness spectrum has been obtained using measurements acquired only from a TRC, and no short wavelength (less than 0.5 m) CAT measurements were available so the short wavelength spectrum from the ballasted track is used. It can be seen that the unevenness level of the slab track is significantly lower than for ballasted track for wavelengths greater than 1 m. This can be attributed to the increased resistance of the slab track to geometry degradation (because of the bending resistance of the slab and the absence of ballast degradation). Moreover, usually softer rail fastenings are used on slab tracks than on ballasted tracks and this can lead to a reduction in the perceived unevenness [28]. Nevertheless, in the wavelength range from 1 m to 0.5 m, the available TRC measurements for both tracks give similar unevenness levels.

Track-ground system properties

The dynamic representation of the two track forms is shown in Fig. 3. All the track systems considered in this study are composed of two UIC60 rails with bending stiffness $E_r I_r$ = 6.42 MN·m^2, hysteretic damping loss factor η_r = 0.01 and mass per unit length m_r = 60 kg/m for each rail. For the ballasted track, the concrete sleepers are considered as rigid bodies with mass m_s = 300 kg and pitching moment of inertia about the x axis I_0 = 200 kg·m^2; the distance between them is d_s = 0.65 m. In the model, the sleeper mass is distributed continuously along the track length. For the slab track, the rails and slab are modelled as infinite Euler-Bernoulli beams. The rail pads are modelled as

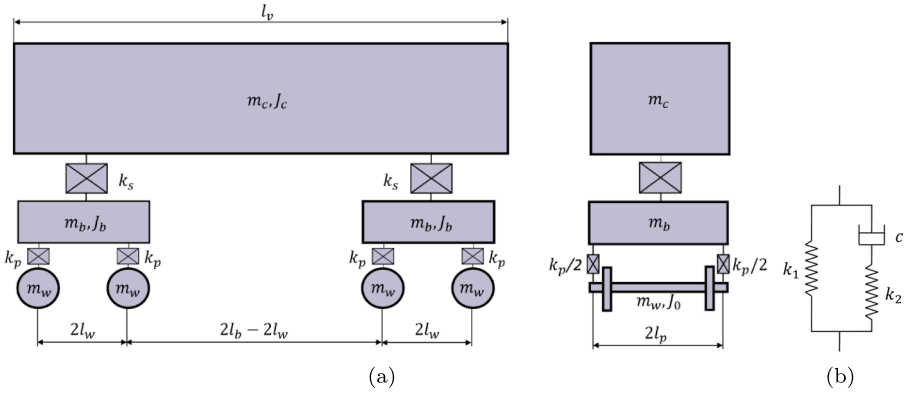

Fig. 1. (a) Vehicle model with primary and secondary suspensions. (b) Suspension model.

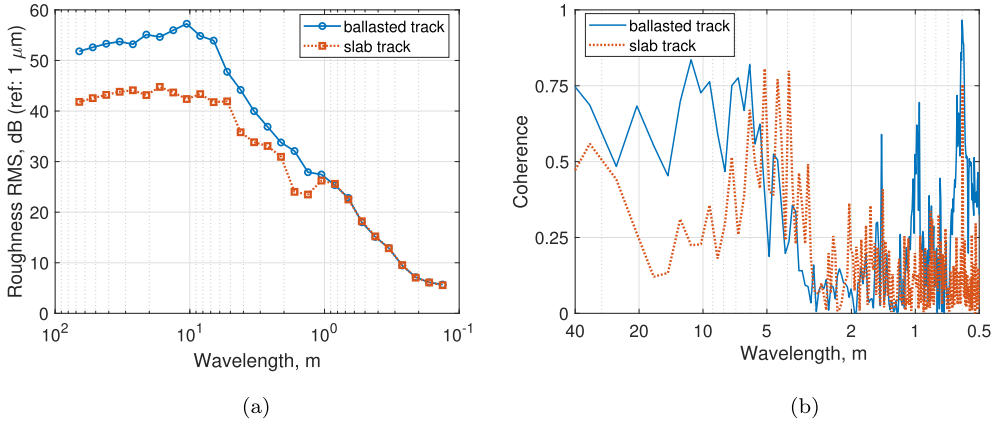

Fig. 2. (a) Unevenness spectra in one-third octave band wavelength and (b) coherence function between left and right rails for ballasted track and slab track [22].

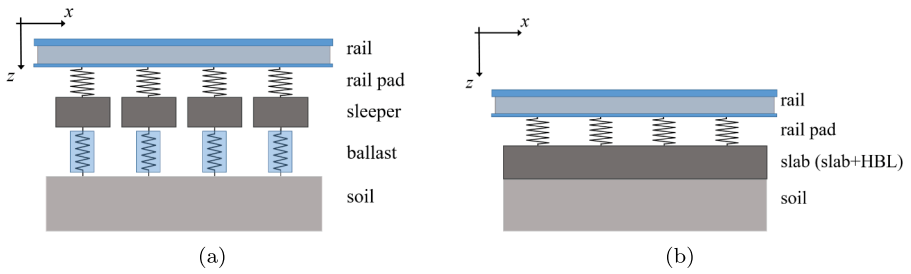

Fig. 3. Beam-spring-mass representation of the track forms. (a) Ballasted track; (b) slab track.

continuous spring elements with negligible mass and hysteretic damping and the ballast is modelled as continuous spring elements with hysteretic damping and consistent mass.

The main resilience of the ballasted track is due to the rail fasteners (i.e. railpads) and the layer of ballast. Four cases with different ballast properties and different railpad stiffnesses are considered with their values given in Table 2. The properties of Case B1 (see Table 2) are largely based on a stiff ballasted track considered in [19]. For Cases B2 and B3, the properties were selected such that the ballast mass for Case B2 is much higher (88%) than Case B1, and the stiffness value for Case B3 is half that of Case B1. Case B4 has the same ballast properties as Case B1 but higher railpad stiffness. For all four cases, the width of the ballast/ground interface strip is $2b = 3.2$ m and the traction variation across the interface area is taken into account by using twelve uniform traction strips, as formulated in [22].

For the slab track, five sets of slab properties are considered. These are given in Table 3 and are mainly based on the specifications of the Rheda 2000 slab track [20] shown in Fig. 4(a). This system [29] is used as a typical example of a monolithic wet-poured slab track. The concrete slab system rests on a hydraulically bonded layer (HBL) that is a mixture of aggregates with a bonding agent, usually cement, and is typically 0.3 m thick (Fig. 4(b)).

For the aims of this study the whole composite slab track system is simplified and modelled as a single beam with mass, bending and torsional stiffness properties (Table 3) of the combined slab and HBL. The contact with the ground has a width $2b = 3.4$ m (Fig. 4(b)) and the traction variation across the interface area is again taken into account by using twelve uniform traction strips. The values of the properties for slab Cases S2 and S3 (see Table 3) were selected such that Case S2 has about 45% of the bending and torsional stiffnesses of Case S1 (i.e. it is assumed that the HBL does not contribute to the bending and torsional rigidities of the slab system) and Case S3 has the same bending stiffness as Case S2 but the mass of the slab is equal to the combined mass of the sleepers and ballast of ballasted track Case B1 (see Table 2). Case S4 has the same mass as Case S1 but the slab has zero bending stiffness while Case S5 is similar to Case S1 but has a softer rail fastening system.

Table 2
Ballast and railpad properties for ballasted tracks.

	Case B1	Case B2	Case B3	Case B4
Railpad stiffness (MN/m)	120	120	120	300
Railpad damping loss factor	0.15	0.15	0.15	0.15
Ballast mass (kg/m)	1740	3258	1740	1740
Ballast stiffness (MN/m^2)	4640	4640	2320	4640
Ballast damping loss factor	0.1	0.1	0.1	0.1

Table 3
Slab track and rail fastener properties.

	Case S1	Case S2	Case S3	Case S4	Case S5
Slab mass (kg/m)	3720.0	3720.0	2201.5	3720.0	3720.0
Slab bending stiffness (MN·m^2)	233.2	103.2	103.2	0	233.2
Slab torsional stiffness (MN·m^2)	339	150	150	339	339
Slab polar moment of inertia (kg·m)	3086	3086	2541	3086	3086
Slab damping loss factor	0.015	0.015	0.015	0.015	0.015
Rail fastener stiffness (MN/m)	120	120	120	120	50
Rail fastener damping loss factor	0.15	0.15	0.15	0.15	0.15

The tracks are located at the surface of a two-layered elastic half-space model that represents a softer soil above a stiffer subgrade. This is a typical soil physical arrangement in which a layer of softer weathered soil about 1–3 m overlies stiffer soil layers. Six different types of ground are selected for this study with the values listed in Table 4. These are defined in terms of their fundamental wavespeeds, the P-wave (or compressional wave) and the S-wave (or shear wave) together with the density. Although not based on actual sites, these properties are chosen as typical examples of what is likely to occur in practice. Ground Types G1 and G2 have been used in [30,22]; they both have a softer layer of depth 3 m overlying a stiffer half-space. Ground Types G3 and G4 have the same layering configuration as Types G1 and G2 but they are considerably softer. For convenience, ground Types G1 and G2 have the same underlying half-space properties; the same wave velocities are used for the underlying half-space of ground Type G4 and the upper layer of ground Types G1 and G3. Ground Type G5 has identical properties with ground Type G1 but the thickness of the upper layer is reduced to 1.5 m. Ground Type G6 is a homogeneous half-space with properties identical with the upper layer of ground Type G1. Note that the S-wave velocities of ground Types G1, G3, G4, G5 and G6 were selected within the speed range of high speed trains in order to allow the effect of critical velocities be studied for the different track forms in Section 'Critical speed for different track forms'.

Loads applied directly on the ground surface – ground dispersion

In order to give insight into the track-ground interaction mechanism and the wave propagation in the ground, the dispersion characteristics of the various ground types are presented in this section. The ground response to a unit load is computed as a function of frequency for the different ground types. Fig. 5(a) shows the dispersion curves for the P-SV (coupled compressional-shear vertical) surface waves of ground Type G1. These are results for the free ground (without the inclusion of the track) and are given for a stationary harmonic vertical point load [31,32]. The vertical response due to a stationary vertical point load is an even function of wavenumber k and thus the response for the negative wavenumbers is not shown in Fig. 5.

Since ground Type G1 is not homogeneous, the P-SV waves are dispersive: the phase velocity of the waves varies with frequency. Fig. 5(a) shows the dispersion diagram (wavenumber-frequency content of the propagating P-SV waves) in the frequency range 0–100 Hz. Lines representing the shear wavenumber of the upper layer ($c_{S1} = 120$ m/s), and the underlying half-space (350 m/s) are also shown. The Rayleigh wavenumber for a homogeneous ground with properties equal to those of the upper layer is also shown. This is calculated [33] as $c_R \approx 109$ m/s (91% of c_{S1}) for Poisson's ratio $\nu_1 = 0.33$.

The dispersion curves plotted in Fig. 5(a) (and the results in Fig. 5(c)) and (d)) were computed by the solution of an eigenvalue

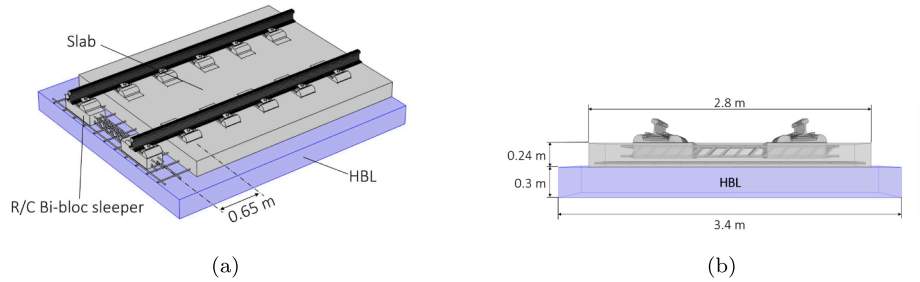

Fig. 4. The Rheda 2000 slab track system [20]. (a) 3D segment of the continuous track and underlying HBL; (b) track cross-section.

Table 4
The parameters used for the different types of ground.

Ground	Layer	P-wave speed (m/s)	S-wave speed (m/s)	Density (kg/m^3)	Damping loss factor	Layer depth (m)
Type G1	Upper layer	240	120	1800	0.1	3.0
	Half-space	700	350	2000	0.1	Infinite
Type G2	Upper layer	500	250	1800	0.1	3.0
	Half-space	700	350	2000	0.1	Infinite
Type G3	Upper layer	240	120	1800	0.1	3.0
	Half-space	400	200	2000	0.1	Infinite
Type G4	Upper layer	120	60	1800	0.1	3.0
	Half-space	240	120	2000	0.1	Infinite
Type G5	Upper layer	240	120	1800	0.1	1.5
	Half-space	700	350	2000	0.1	Infinite
Type G6	Half-space	240	120	1800	0.1	Infinite

problem [4,34,35]. This eigenvalue problem is transcendental and has an infinite number of solutions, and must be solved with search techniques. This procedure is computationally expensive and sometimes can lead to local optima or problems identifying certain solutions. An alternative approach is to plot the P-SV Green's function (response to a unit vertical harmonic load) of the soil as a contour plot against frequency and radial wavenumber. This is shown in Fig. 5(b). This exhibits peaks that reveal the presence of the surface waves. The largest peak corresponds to the dominant surface wave. The lines representing the P-SV propagating waves shown in Fig. 5(a) are also superimposed in

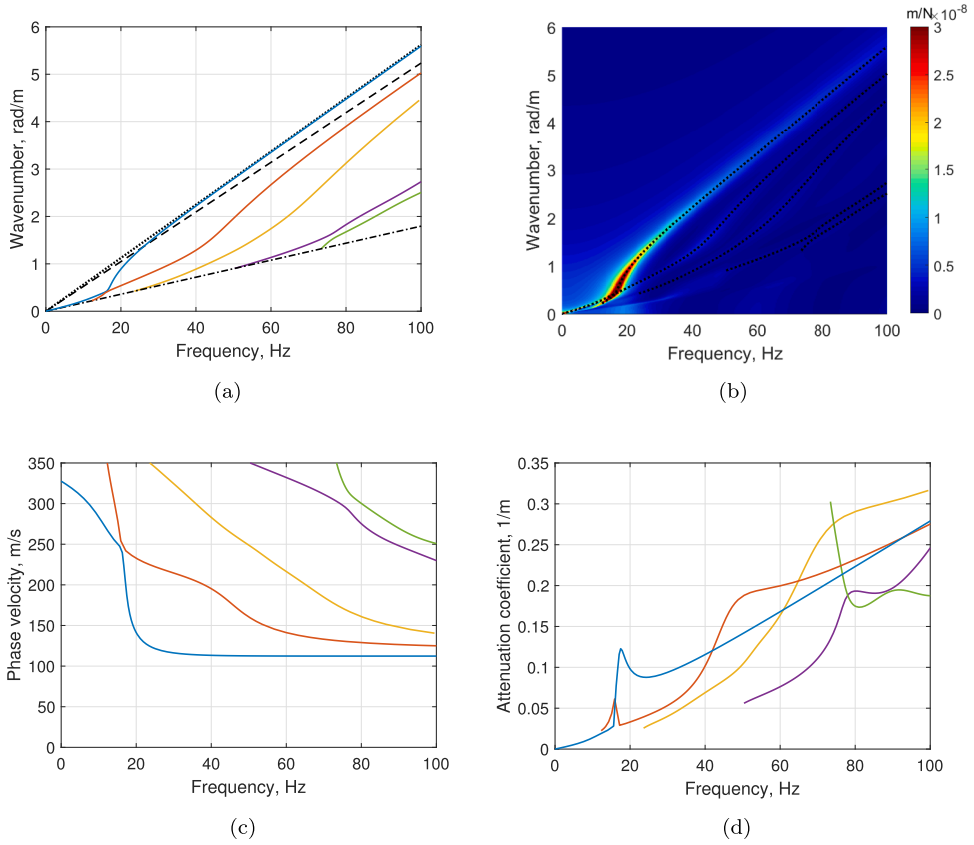

Fig. 5. Characteristic curves for P-SV waves on ground Type G1: (a) Dispersion diagram with propagating P-SV waves (——); shear wave speed of upper layer (- - -), shear wave speed of underlying half-space (– · – ·), and Rayleigh wave speed of upper layer material (·····). (b) Contour plot of the vertical displacement (m/N) in the frequency-wavenumber domain. (c) Phase velocity and (d) Attenuation coefficient of the P-SV waves.

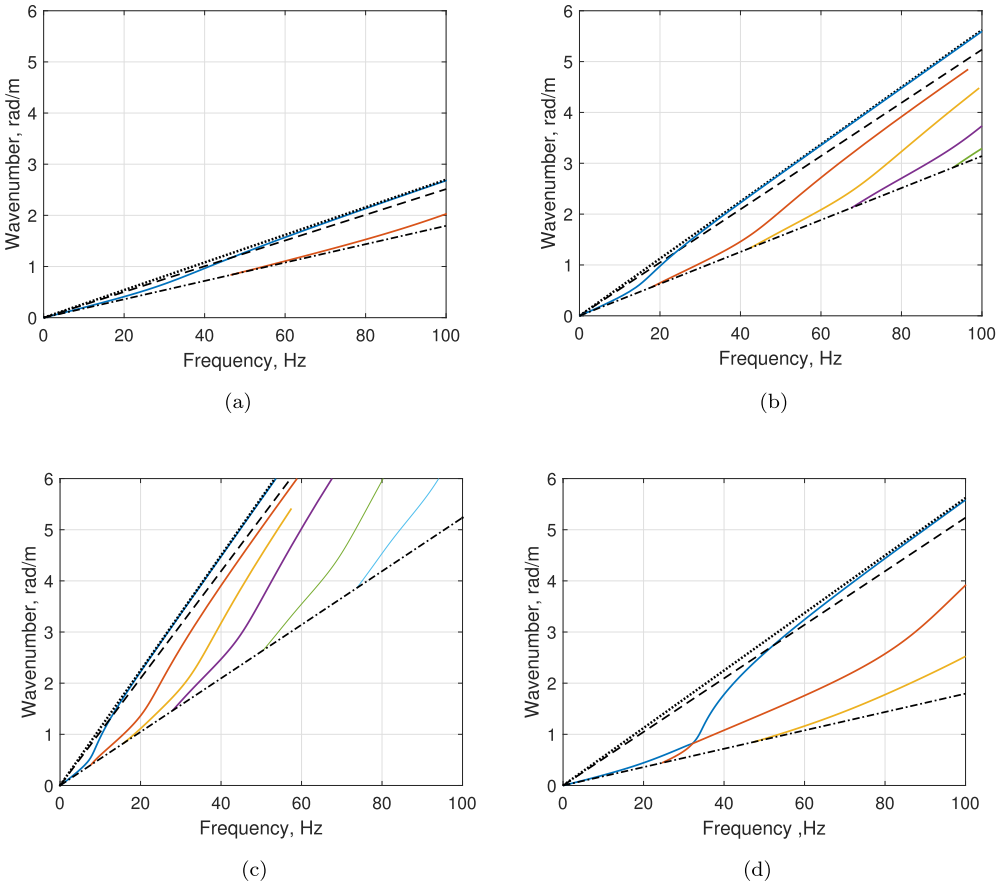

Fig. 6. Dispersion diagrams with propagating P-SV waves (——); shear wave speed of upper layer (- - -), shear wave speed of underlying half-space (–·–·), and Rayleigh wave speed (·····): Ground (a) Type G2; (b) Type G3; (c) Type G4; (d) Type G5.

Fig. 5(b). Although not all surface waves of the layered half-space can be identified, those that dominate the response due to a vertical load at the soil surface can be clearly seen.

Fig. 5(c) shows the phase velocity of each wave, given by $c = \omega/k$. At very low frequencies only a single propagating mode exists which has a wave speed close to that of the shear waves in the underlying half-space (350 m/s). At around 12.3 Hz the first 'cut-on' frequency of this layered ground occurs. Above this frequency, the first wave propagates mainly in the upper layer with little influence of the underlying half-space and the wave speed tends towards the speed of Rayleigh waves in the upper layer (109 m/s). Subsequent modes cut on at 23.6 Hz, 50.4 Hz and 73.4 Hz. The phase velocity of these higher modes varies between the shear wave velocity of the underlying halfspace (at the cut-on frequency of the mode) and the shear wave velocity of the top layer.

Fig. 5(d) shows the vibration attenuation rates of the propagating surface waves. These are obtained from the imaginary part of the complex wavenumber k[35].

The dispersion curves of ground Types G2, G3, G4 and G5 are presented in Fig. 6. The first few 'cut on' frequencies for each case are listed in Table 5. Comparing ground Types G1 and G2, that have the same properties for the underlying half-space, the 'cut on' frequencies increase significantly with the increase of the wave velocities in the upper layer (see Table 4). This is expected since the S-waves correspond to motion that involves mostly deformation of the upper layer. Comparing ground Types G1 and G3, that have the same properties for the upper layer, ground Type G1 that has a stiffer underlying half-space shows lower values of the 'cut on' frequencies. Additionally, the intensity of the surface waves is expected to be higher for ground Type G3, with the softer underlying substratum, than for ground Type G1. This can be seen in Fig. 7 in which the real part of the vertical and lateral displacement is plotted against depth for an excitation frequency of 10 Hz and wavenumber $k = 0.52$ rad/m that corresponds to a phase velocity of 120 m/s. This shows that the energy is largely transmitted in the top 3 m soft layer of soil and that ground Type G3 contains considerably more motion of the underlying half-space.

Table 5
The 'cut on' frequencies of the first four P-SV waves for the different ground types.

Ground	'Cut on' frequency (Hz)				
	Type G1	Type G2	Type G3	Type G4	Type G5
Mode 1	12.3	46.4	18.0	7.6	24.6
Mode 2	23.6	106.8	42.3	16.0	47.2
Mode 3	50.4	167.0	67.7	28.0	100.7
Mode 4	73.4	227.0	92.9	50.5	146.8

Ground Type G5 has identical material properties to ground Type G1 but half the depth for the upper layer; as seen in Table 5 the values of the 'cut on' frequencies are double the values for ground Type G1. Moreover, the intensity of the surface waves is expected to be lower for ground Type G5 especially at lower frequencies. This is confirmed by in Fig. 7 where the real part of the vertical and lateral displacement of ground Type G5 has significantly lower values at the surface and the motion is mostly contained in the top 1.5 m instead of the 3 m depth for ground Type G1.

Fig. 8 shows the transfer receptances at two different distances on the free ground surface for a stationary harmonic point load. These are calculated with an inverse Fourier transform (or they could be calculated with an equivalent Hankel transform, [31,32]) from the Green's functions that have been calculated in the wavenumber domain. For all five ground types, a broad peak occurs in the transfer receptance at low frequencies. The peak occurs at about 18 Hz for ground Type G1, 35 Hz for ground Type G2, 17 Hz for ground Type G3, 9 Hz for ground Type

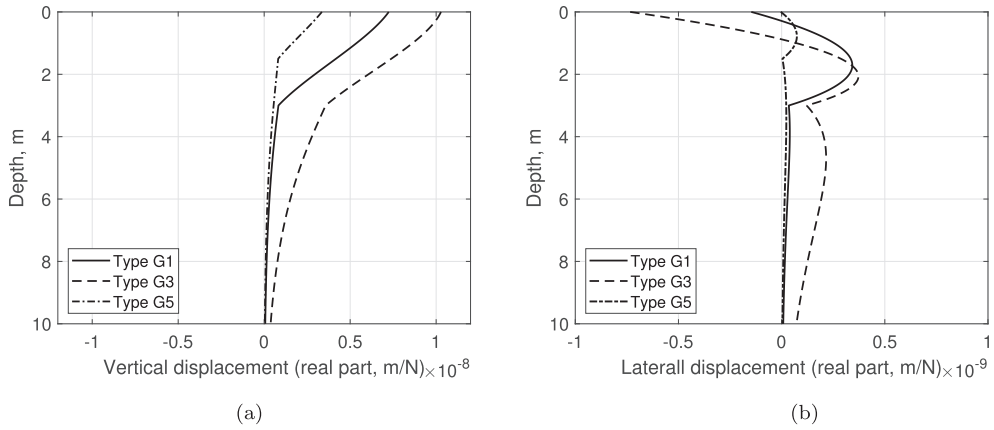

Fig. 7. Real part of the P-SV modes at 10 Hz and for wavenumber $k = 0.52$ rad/m (120 m/s phase speed) for ground Type G1, ground Type G3 and ground Type G5. (a) Vertical displacement; (b) lateral displacement.

G4 and 35 Hz for ground Type G5. These peaks correspond approximately to the 'cut on' frequencies of the layered ground (see Table 5). The transfer receptances for ground Types G1, G2 and G5 are equal at low frequencies, where the vibration propagation is dominated by the underlying half-space, this having identical properties for the three grounds. The results start to differ at higher frequency, with ground Type G1 having a higher receptance above 6 Hz as waves start to cut on in the upper layer. For the thinner upper layer of ground Type G5 waves start to cut on in the layer above 17 Hz. Conversely, ground Types G1 and G3 have different transfer receptances at low frequencies due to the differences in their underlying half-space but this difference reduces above their 'cut on' frequencies.

Ground dispersion for different track forms and the effect of load speed

For a moving load a single radial wavenumber can no longer be used in the calculation of the receptances. If the load is moving on a straight line, the wave field is transformed into the domain of two wavenumbers, k_x parallel to the movement of the load and k_y perpendicular to it.

By working in a frame of reference moving with the load [24], the steady-state response for a harmonic load of frequency ω in the wavenumber-frequency domain is given as $\tilde{\mathbf{u}}(k_x, k_y, z, \hat{\omega})$ that is time harmonic with amplitude $\tilde{\mathbf{u}}(k_x, k_y, z)$ and response frequency $\hat{\omega} = \omega - k_x v$. This frequency may take negative values; as a consequence each loss factor, η, in the ground layers or in the track components should take the form of $\eta \text{sign}(\hat{\omega})$. The steady state response consists of an infinite number of spatially harmonic components, each of which is time harmonic, with frequency and amplitude which are dependent on the corresponding wavenumber [24].

Results are presented for the track receptance as a function of frequency $\omega/2\pi$ for ballasted track Case B1 and slab track Case S1. The systems are subjected to a series of moving unit amplitude sinusoidal excitations applied symmetrically on both rails. Fig. 9 shows the receptance of the rail at the moving excitation point as a contour wavenumber-frequency representation for the ballasted track Case B1 and the slab track Case S1 on ground Type G1. The load speed is $v = 33.3$ m/s (120 km/h).

From Fig. 9 it is clear that the response due to the movement of the load is not symmetric with respect to wavenumber $k_x = 0$. This occurs because the response frequency $\hat{\omega} = \omega - k_x v$ varies with wavenumber k_x, resulting in a skewness of the calculated response compared with the non-moving case. The dominant response in Fig. 9 occurs at smaller wavenumbers behind of the load (positive wavenumbers) than ahead of it [24]. This is not the case for the response with respect to the wavenumber k_y; the load movement does not affect the symmetry about the x-axis so the dominating surface waves will have phase velocities similar to the P-SV waves of the fixed load case shown in Fig. 5(b).

With the inclusion of the ballasted track no waves with wavenumbers above about 2 rad/m can propagate along the track at these frequencies; for the slab track the corresponding limit is about 1 rad/m. The difference in these maximum wavenumbers is because of the increased bending stiffness of the slab track compared with the ballasted track. The ballasted track also shows higher values of maximum response, although the difference is not clearly visible from the contour plots. Due to the low resilience of the two tracks the response at the ground surface at the track centreline is similar to the rail response in

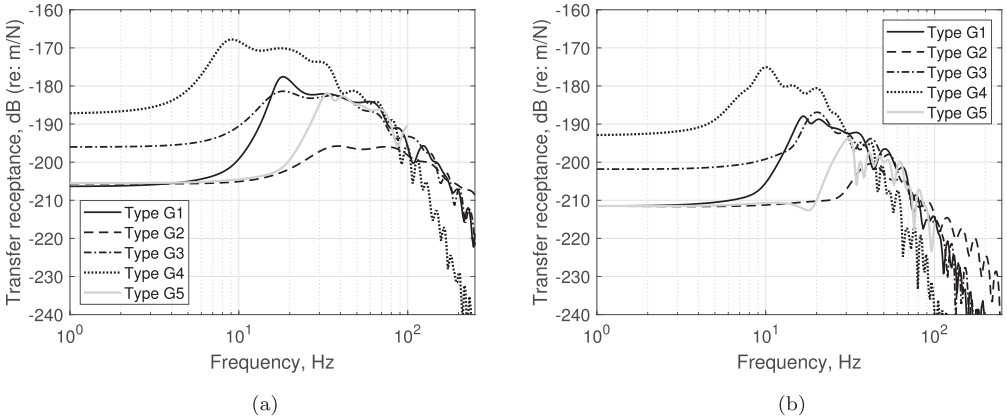

Fig. 8. Transfer receptances for the five different ground types. (a) 8 m from the source; (b) 16 m from the source.

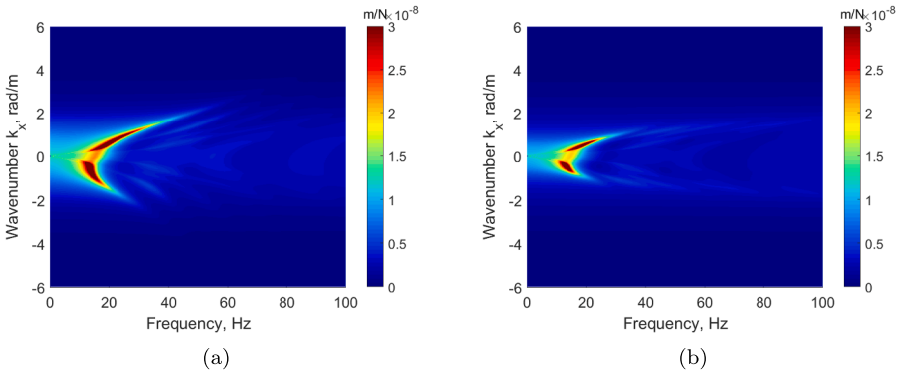

Fig. 9. Contour plots of the rail point receptance in the frequency-wavenumber domain for tracks on ground Type G1 due to moving harmonic loads at $v = 33.3$ m/s with respect to wavenumber k_x. (a) Ballasted track Case B1; (b) slab track Case S1.

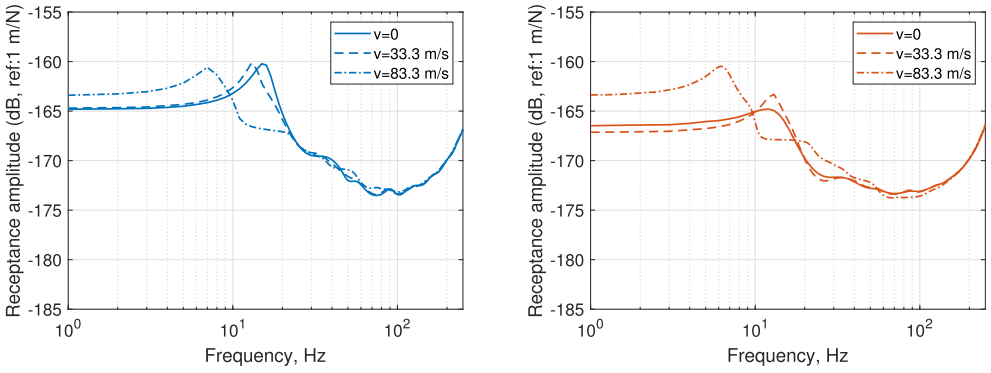

Fig. 10. Rail receptance magnitude for ground Type G1 due to stationary ($v = 0$) and moving ($v = 33.3$ and $v = 83.3$ m/s) excitation: (a) ballasted track Case B1; (b) slab track Case S1.

Fig. 9.

Fig. 10 compares the rail point receptance magnitude for $v = 0$ with that for load speeds $v = 33.3$ m/s and 83.3 m/s (300 km/h); results are again shown for ballasted track Case B1 and slab track Case S1. These are calculated by a wavenumber inverse Fourier transform at the load point ($x = 0$). Thus the lines shown for load speed 33.3 m/s for the two track forms in Fig. 10 result from an inverse Fourier transformation at $x = 0$ of the complex wavenumber response shown in Fig. 9.

Comparing the rail receptance magnitude between the two track forms in Fig. 10 it can be seen that, for $v = 0$ and 33.3 m/s, the ballasted track shows about 3 dB higher vibration levels than the slab track. However, for a load speed of 83.3 m/s both ballasted and slab tracks show similar point receptances. The peak value of the receptance occurs at about the same frequencies for both track forms. As the load speed increases, the peak of the rail receptance tends to shift to lower frequencies.

For a harmonic load moving with a constant velocity, vibration at an observation point in the track/ground can be also considered as harmonic if the point is moving in the same direction and speed as the moving load. For such a case of a moving frame, the transfer functions (Green's functions) between the excitation points at the wheel-rail interface and the observation point are time-invariant. The results presented in Figs. 9 and 10 show the dynamic response of the rail using such moving Green's functions.

However, the Green's functions between a moving excitation point and a fixed observation point are dependent on time. This is due to the fact that, for a receiver at a fixed position in the free field, the vibration level depends on the position of the load along the track that is dependent on time. Since the load moves, a load of a single frequency in the moving frame of reference will produce a transient response at a fixed point in the ground or the track which has a spectrum containing a range of frequency components, i.e., a Doppler shift occurs depending on the speeds of wave propagation in the track/ground. The response amplitude is also time-dependent.

Fig. 11 shows the cumulative ground response (displacement) spectrum due to a unit load (symmetrically distributed on the two rails) for the same range of excitation frequencies (1–250 Hz). The cumulative response spectrum is defined here as $\int_{-\infty}^{\infty} |u(y,f)|^2 df$ and is obtained for 250 logarithmically spaced excitation frequencies $f = \omega/2\pi$. Results are shown for load speeds 33.3 m/s and 83.3 m/s for receivers at $y = 8$ m and 16 m from the track centreline. The vibration level rises to a peak at about 17 Hz for both speeds. As in the stationary transfer receptance shown in Fig. 8, this rise in level is associated with the cut-on of waves localised in the upper surface layer of the soil. The trends in Fig. 11 are similar to those for ground Type G1 in Fig. 8; however, with the track included the vibration in Fig. 11 drops faster at high frequency. The results for the two track forms in Fig. 11 show the same vibration characteristics for frequencies below 15 Hz. Above 15 Hz, the cumulative response shows lower levels for the case of the slab track, with a difference of around 1 dB at the peak at 17 Hz increasing to around 4 dB at high frequency.

Fig. 12 shows corresponding results for a case where the loading is not symmetrically distributed on the two rails and the track is allowed to rotate around the x axis. This shows the cumulative response spectrum for harmonic unit loads on the two rails in anti-phase. Lower response levels can be seen for both tracks in the low frequency range

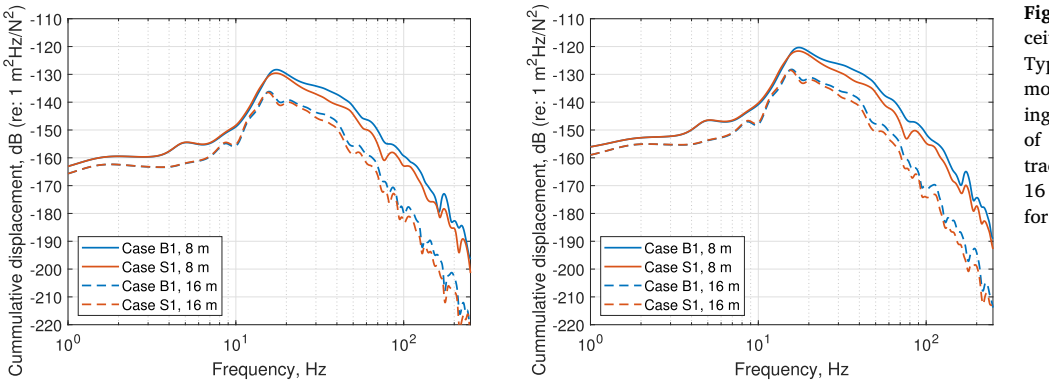

Fig. 11. Cumulative ground response (receiver) spectrum in the far field for ground Type G1. Response due to moving harmonic and symmetrically distributed loadings of unit force amplitude on the two rails of the ballasted track Case B1 and slab track Case S1 at 8 m from the track and 16 m from the track: (a) for 33.3 m/s; (b) for 83.3 m/s.

below 15 Hz than those in Fig. 11. Above 15 Hz, the response due to the anti-symmetric loading increases to the same level as the symmetric case, with a peak around 20 Hz. At higher frequency it remains about 5 dB higher than the symmetric case.

Ground vibration due to train passages

In this section, the MOTIV model is used to investigate the effects of different track forms on the vibration levels of the ground and the track during a train passage. The response is calculated for the full passage of a train of four vehicles with properties given in Table 1; two train speeds are considered, 33.3 m/s and 83.3 m/s. Initially the unevenness spectrum of the ballasted track shown in Fig. 2 is applied for both ballasted tracks and slab tracks in order to enable a nominal comparison of the two track forms based on their structural performance. The unevenness spectrum of the slab track shown in Fig. 2 is applied only for the slab track simulations in Section 'The effect of the track alignment'. The correlation between the two rails [22] (Fig. 2(b)) is included by using the available TRC measurement in the wavelength range 35–0.5 m. For wavelengths longer than 35 m the unevenness between the two rails is considered as fully correlated, whereas for wavelengths shorter than 0.5 m it is considered as uncorrelated [22].

Vibration level at the ground surface

The vertical vibration velocity level at the ground surface due to the passage of the train on ballasted track B1 and slab track S1 is shown in Fig. 13. The results are shown as the average one-third octave band spectrum at 8 m and 16 m from the track centreline during the train passage. The response shown includes the contribution of both the quasi-static excitation (due to the moving axle loads) and the dynamic excitation (due to the rail unevenness).

The vibration level rises to a broad peak between 16 and 63 Hz at 33.3 m/s and between 25 and 100 Hz at 83.3 m/s. This is associated with the cut-on of waves localised in the upper surface layer of the soil. Comparing the vibration spectra at the two different distances, it can be seen that the response decays significantly with distance. The decay with distance is similar for both train speeds and is more prominent below about 3 Hz, where the quasi-static contribution is expected to dominate the response, and above 12.5 Hz. Higher vibration levels are found for the higher speed (83.3 m/s) in most one-third octave bands. This is mainly due to the shape of the unevenness spectrum; for a given frequency the corresponding unevenness shifts towards longer wavelengths that have higher unevenness levels (see Fig. 2).

The differences between the results for the two track types in Fig. 13 are relatively small. However, larger differences are found in the quasi-static component, as shown in Fig. 14. The slab track has much lower levels of quasi-static component above 3 Hz for 33.3 m/s and 8 Hz for 83.3 m/s due to the influence of the slab bending stiffness. Nevertheless due to the dominance of the dynamic excitation apart from very low frequencies, this difference does not affect the overall vibration levels at these distances.

The effect of the ground conditions

Fig. 15 shows the level differences in dB between the total vibration for the two track types. These are shown as the level for slab track S1 minus that for ballasted track B1. The results are given for three ground types at 8 m from the track centreline. In each case the vibration level for the slab track is less than 3 dB lower than that for the ballasted track

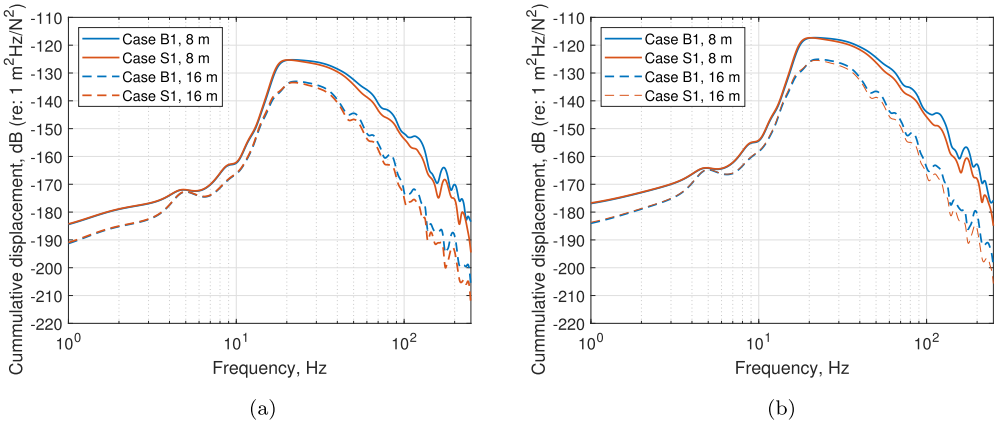

Fig. 12. Cumulative ground response (receiver) spectrum in the far field for ground Type G1. Response due to anti-phase moving harmonic unit force amplitude on each rail of the ballasted track Case B1 and slab track Case S1 at 8 m from the track and at 16 m from the track: (a) for 33.3 m/s; (b) for 83.3 m/s.

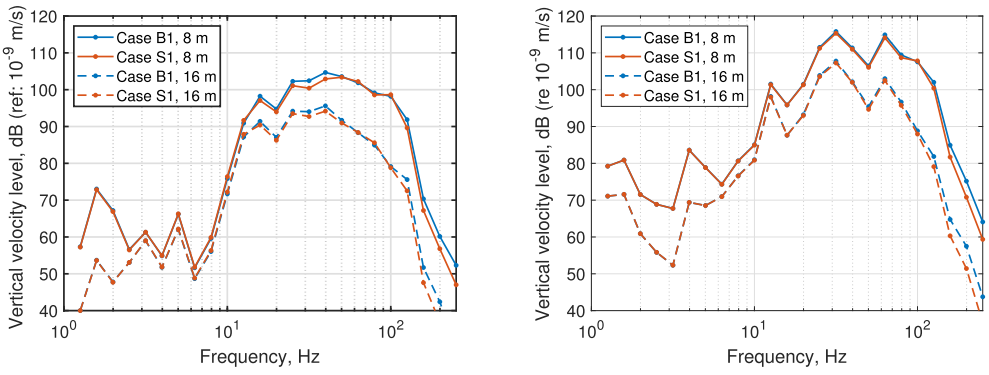

Fig. 13. Total ground response level in one-third octave bands of ballasted track Case B1 and slab track Case S1 at 8 m and 16 m from the track for train speed: (a) 33.3 m/s and (b) 83.3 m/s.

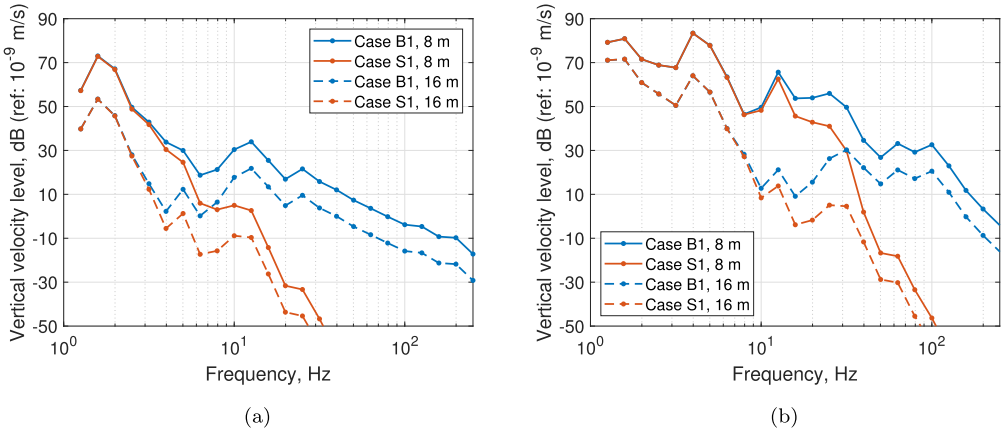

Fig. 14. Quasi-static ground response level in one-third octave bands of ballasted track Case B1 and slab track Case S1 at 8 m and 16 m from the track for train speed: (a) 33.3 m/s and (b) 83.3 m/s.

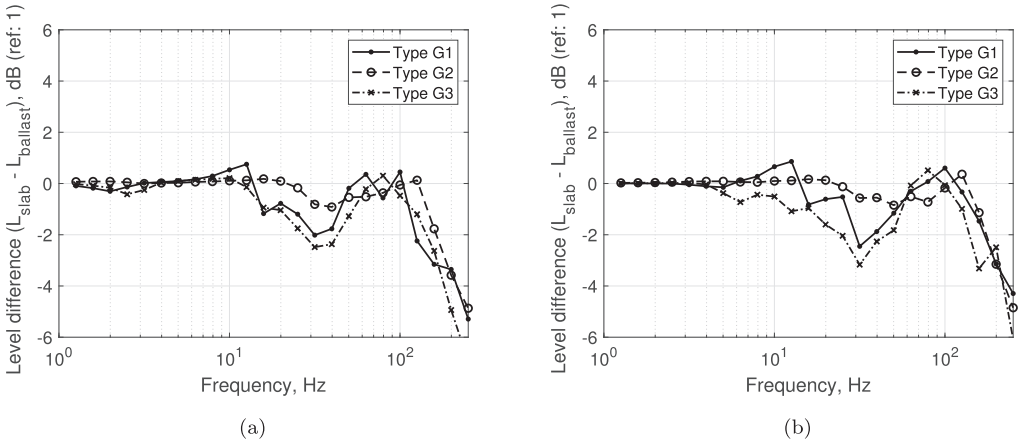

Fig. 15. One-third octave level differences of slab track Case S1 minus ballasted track Case B1 on ground Type G1, ground Type G2 and ground Type G3 at 8 m from the track centreline for train speed: (a) 33.3 m/s and (b) 83.3 m/s.

between about 20 and 50 Hz. Above 100 Hz the level for the slab track is progressively lower as frequency increases. The results are similar for ground Types G1 and G3; as these have the same upper layer of soil this suggests that the differences are dominated by this surface layer. For ground Type G2, which has a stiffer surface layer, the level differences are smaller. The results for larger distances from the track are similar.

The results from the two track forms are similar in the frequency bands 63–100 Hz. This corresponds to the resonance frequency of the combined rail and unsprung mass on the track stiffness, at which the interaction force has a maximum [12]. This can be identified from Fig. 16 as the frequency at which the rail and wheel receptances have similar magnitudes, which occurs at about 80 Hz. In this frequency region, the rail receptances are similar for both track types, Case B1 and Case S1, and are only affected by the ground below 25 Hz. Moreover, the rail receptances are unaffected by load speed above about 20 Hz for the ballasted track and 40 Hz for the slab track, as shown in Fig. 10. Fig. 16 also shows the rail receptance magnitude for ballasted track B4 and slab track S5 that will be discussed further in Section 'The effect of

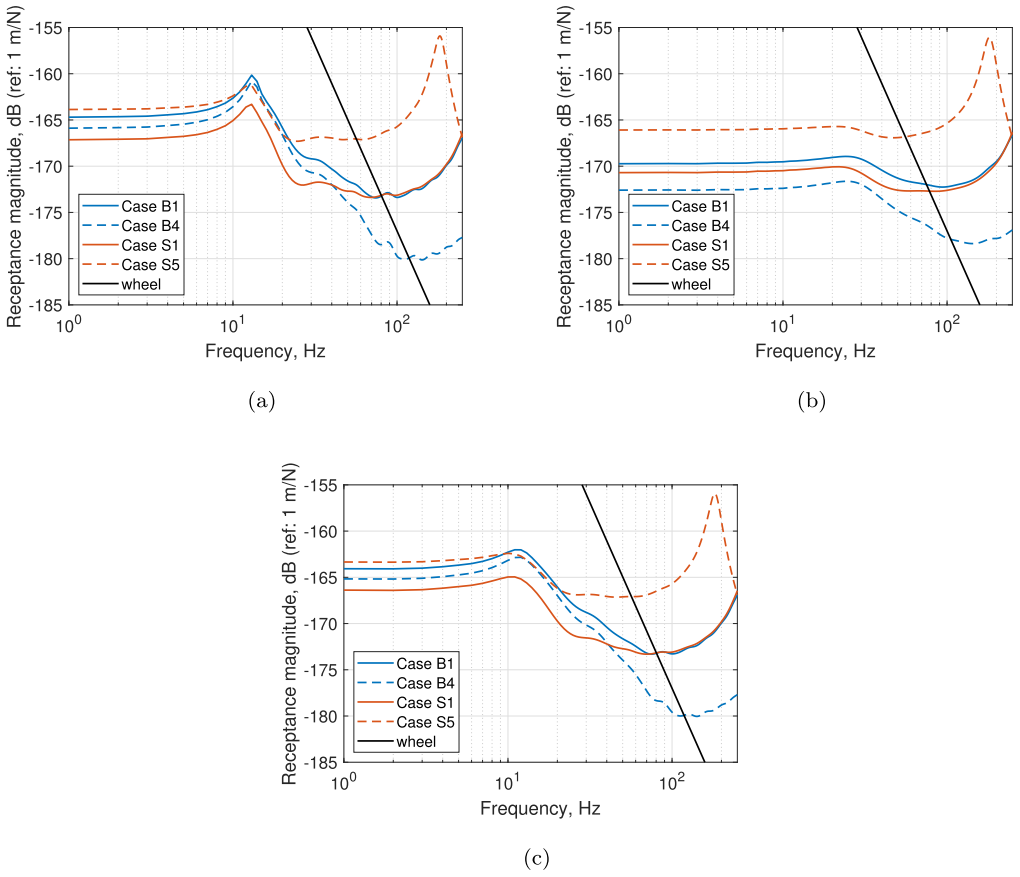

Fig. 16. Magnitude of wheelset point receptance and rail point receptance for ballasted track B1, ballasted track B4, slab track S1 and slab track S5 due to loading moving at $v = 33.3$ m/s for (a) ground Type G1, (b) ground Type G2 and (c) ground Type G3.

the fastening system'. For slab track S5, the resonance of the rail mass on the corresponding soft railpad support stiffness ($k_p = 50$ MN/m) can be clearly seen at about 185 Hz.

To highlight the resonance frequency of the rail and unsprung mass on the track stiffness, Fig. 17 shows the displacement of the rail and the wheel at the first wheel/rail contact point due to a unit magnitude rail unevenness. This is distributed on both rails and applied in phase. These results are for ground Type G1 and for the ballasted tracks B1 and B4 and the slab tracks S1 and S4. The displacements at the other wheel/rail contact points show similar trends.

The peaks in Fig. 17(a) occur at about 80 Hz for ballasted track B1, 120 Hz for ballasted track B4, 80 Hz for slab track S1 and 55 Hz for slab track S5. These frequencies are consistent with the rail/wheel receptance intersection points in Fig. 16(a). Slab track S1 has lower rail displacement than ballasted track B1 for frequencies below 50 Hz due to its lower point receptance. In the frequency range of the resonance 50–100 Hz, the slab track has higher levels of vibration due to its lower damping. Above 100 Hz both tracks show similar vibration levels.

The effect of the track mass

One difference between the two track forms is that the slab track has a higher mass than the ballasted track. To investigate the effect of this, Fig. 18 shows the vibration levels of various track types relative to that

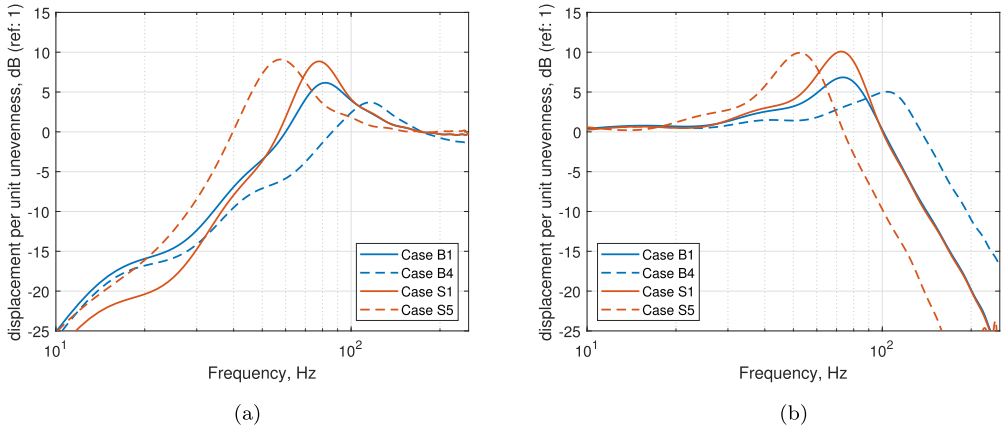

Fig. 17. Magnitude of (a) rail and (b) wheel displacements for unit rail unevenness. Ballasted track B1, ballasted track B4, slab track S1 and slab track S5 due to loading moving at $v = 33.3$ m/s for ground Type G1.

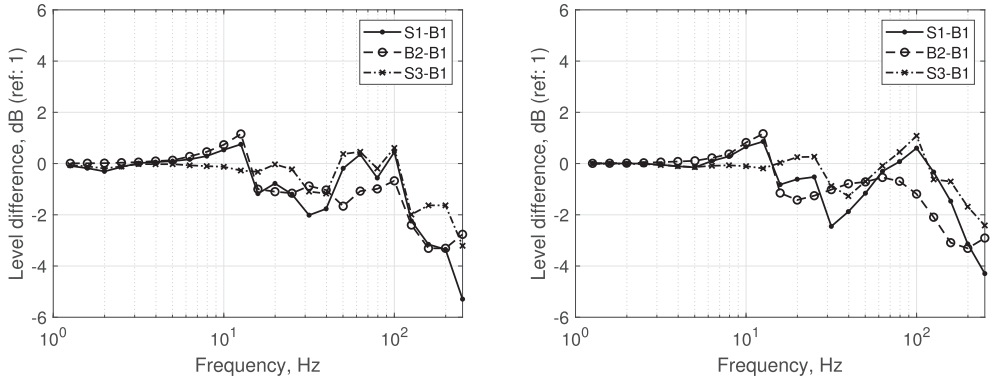

Fig. 18. One-third octave level differences, relative to ballasted track B1, of slab track S1, ballasted track B2 and slab track S3; all for ground Type G1 at 8 m from the track centreline for train speed: (a) 33.3 m/s and (b) 83.3 m/s.

of ballasted track B1.

Ballasted track B2 and slab track S1, which have greater mass than the reference track, both show lower vibration levels. This suggests that the main reason for the level differences seen in Fig. 15 is the higher mass of the slab track rather than its bending stiffness. Conversely, ballasted track B1 and slab track S3, which have the same mass, show similar vibration levels up to about 100 Hz. Above 100 Hz, the reduced stiffness of the ballast for Case B1 seems to lead to higher vibration levels.

The effect of ballast stiffness and slab rigidity

The ballast layer for ballasted track B3 has the same mass but half the stiffness of ballasted track B1. Fig. 19(a) shows the level difference between these two tracks. They show the same levels for all one-third octave frequency bands up to 125 Hz. Above 125 Hz, the reduced stiffness of the ballast for Case B3 leads to higher vibration levels.

To show the effect of the slab bending stiffness, Fig. 19(b) also compares the results for two slab track variants with reduced bending stiffness; these results are shown relative to slab track S1. Slab tracks S1 and S2 have very similar vibration levels at all frequencies despite the fact that track S2 has 45% lower bending stiffness. Slab track S4 which has zero bending stiffness gives slightly lower vibration levels than the other slab tracks but the differences are less than 2 dB in all frequency bands.

The effect of the fastening system

In the comparisons presented in the previous sections all ballasted and slab track cases had the same rail fastener stiffness (k_p = 120 MN/m). In practice, a softer rail fastening is generally used on slab tracks than on ballasted tracks to compensate for the ballast stiffness. Fig. 20 shows the level difference between the results for slab track S5 with a fastener stiffness of k_p = 50 MN/m and ballasted tracks B1 and B4 (the latter with railpad stiffness k_p = 300 MN/m, see Table 4).

A slight rise in vibration of the slab track occurs around 40–63 Hz but at 80 Hz and above the vibration level is considerably reduced due to the soft fasteners. These ground vibration level differences are more pronounced for the comparison between the slab track and the ballasted track B4 with stiffer railpads. The rise in level around 40–63 Hz can be attributed to the higher rail rec eptance due to the reduced track stiffness. As a result the resonance of the unsprung mass on the track stiffness shifts to around 55 Hz as can be seen in Fig. 16(a).

The effect of the track alignment

In Fig. 2 it was shown that the measured unevenness level of the slab track is significantly lower than the ballasted track for wavelengths longer than 1 m. However, in the comparisons presented in the previous sections, all cases had the same nominal track unevenness which was based on a measurement of a ballasted track. Fig. 21 shows the results for slab track S1 obtained using the measured track unevenness levels

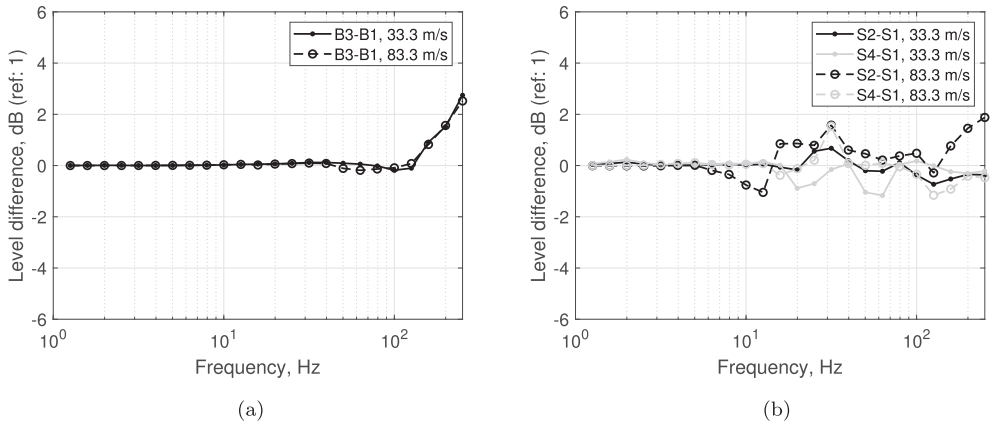

Fig. 19. One-third octave level difference of (a) ballast track B3 relative to ballasted track B1 and (b) slab track S2 and slab track S4 relative to slab track S1. Results for ground Type G1 at 8 m from the track centreline and train speed 33.3 m/s and 83.3 m/s.

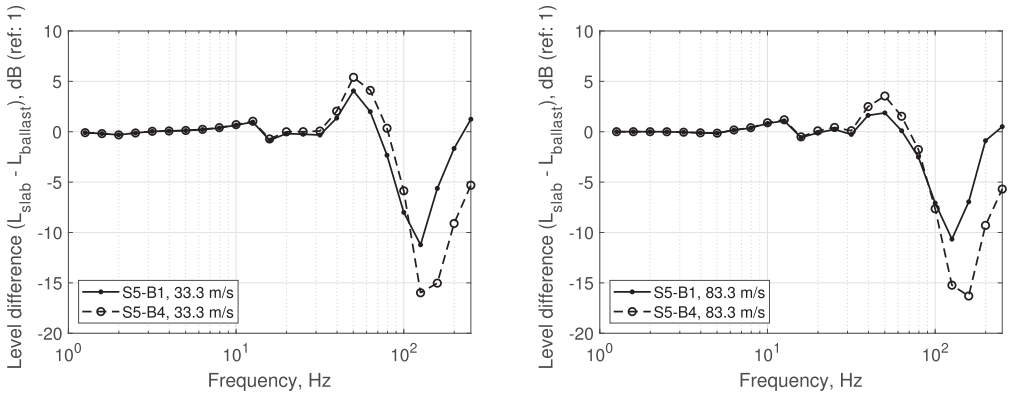

Fig. 20. One-third octave level difference of slab track S5 relative to ballasted track B1 and ballasted track B4 at 8 m from the track centreline on ground Type G1 for train speed: (a) 33.3 m/s and (b) 83.3 m/s.

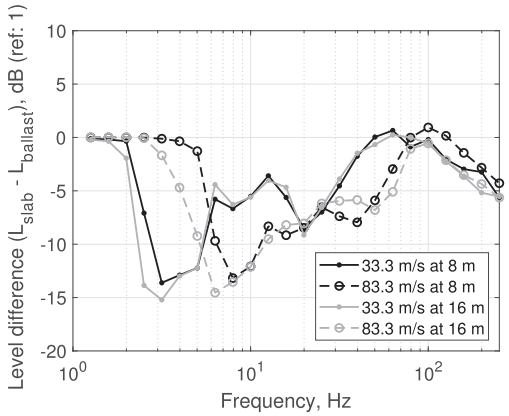

Fig. 21. One-third octave spectra level difference of slab track Case S1 relative to ballasted track Case B1 due to different rail unevenness levels (Fig. 2) for train speed 33.3 m/s and 83.3 m/s and distance from the track 8 m and 16 m.

for the slab track. These are shown relative to ballasted track B1 with the track unevenness levels for the ballasted track.

For a train speed of 33.3 m/s the vibration level of the slab track is significantly lower in the frequency range 2.5–40 Hz. For 83.3 m/s the reduction is shifted to the frequency range 5–63 Hz. The upper limit of this frequency range corresponds to unevenness wavelengths of about 1 m for both train speeds. Above that frequency, the two track forms show similar ground vibration levels. However, above 100 Hz, as frequency increases the vibration level for the slab track is progressively lower even for the same unevenness (see Fig. 15). Below about 3 Hz the response is dominated by the quasi-static response which is similar for both track forms, as shown in Fig. 14.

Critical speed for different track forms

Large amplitude track deflections are generated when trains travel with speeds close to the wave velocity of the supporting track-ground system. This is known as the critical velocity effect and has safety implications; it can also result in a significant increase in the need for track maintenance due to subgrade deterioration. In this section simulation results are presented of track deflection as a function of speed for different track forms from which the critical velocity can be identified.

Fig. 22 shows the maximum rail displacement due to a unit constant load equally distributed on the two rails and moving at a large range of speeds. The results in the four graphs are for four ground types with properties given in Table 4. In each case results are presented for four different track forms with the track properties given in Tables 2 and 3. The first two are ballasted track B1 and slab track S1. The third is ballasted track B2, which has a higher ballast mass than ballasted track B1, so that the combined sleeper and ballast mass is equal to the mass of slab track S1. The fourth track form is the slab track S4 with the same mass properties as slab track S1 but zero bending stiffness of the slab.

In each graph in Fig. 22 the critical speed can be identified by a large increase in the track deflection. Comparing the critical speed for the four different ground types it seems that it mostly depends on the properties of the surface layer of the ground. Ground Type G1 in Fig. 22(a) and ground Type G3 in Fig. 22(c), which have the same properties for the upper layer, show similar maximum rail responses for all speeds and consequently similar peak-response load speeds. For ground Type G2 in Fig. 22(b), which has a much stiffer upper ground layer, the maximum rail response is considerably lower for all load speeds and the critical speed is much higher than for ground Type G1. Ground Type G4 in Fig. 22(d), which has both a softer upper layer and a softer underlying half-space than the other three ground types, shows the highest values of maximum rail response at all speeds and the lowest critical speeds.

Comparing the results in Fig. 22 for the different track forms, slab track S1 has a higher critical speed than the other track forms for all ground types. Moreover, its maximum rail response is lower than that of the other track forms for all speeds below the critical speed. The results for ballasted track B1 and slab track S1 are summarised in Table 6 for six ground types. This shows the values of critical speed along with the dynamic amplification factor, which is the ratio of the maximum rail displacement at the critical speed to the static rail response. The values of the Rayleigh wave speeds of the surface layer [33] are also given for all the ground types.

From the curves in Fig. 22 and the values listed in Table 6 it can be seen that the critical speeds for the ballasted track are close to the Rayleigh wave speeds of the surface layer for ground Types G1, G2, and G3. For the softer ground Type G4 the critical speed seems to be 20% higher than the Rayleigh wave speed of the upper ground layer. For slab track S1, the critical velocities are considerably higher than those for ballasted track B1; this is due to the bending stiffness of the track slab. The increase seems to be greater for the ground types with softer surface layers. For the other two track forms shown in Fig. 22, the values of the critical speeds seem to be slightly lower than the values estimated for ballasted track B1, whereas the maximum rail displacement is similar for all these three tracks.

Further results are given in Fig. 23 to show the effect of ground layering. In each graph results are shown for ground Type G1, which has a layer thickness of 3 m, ground Type G5 with a layer thickness of 1.5 m and ground Type G6 which is a homogeneous ground. All ground properties are given in Table 4.

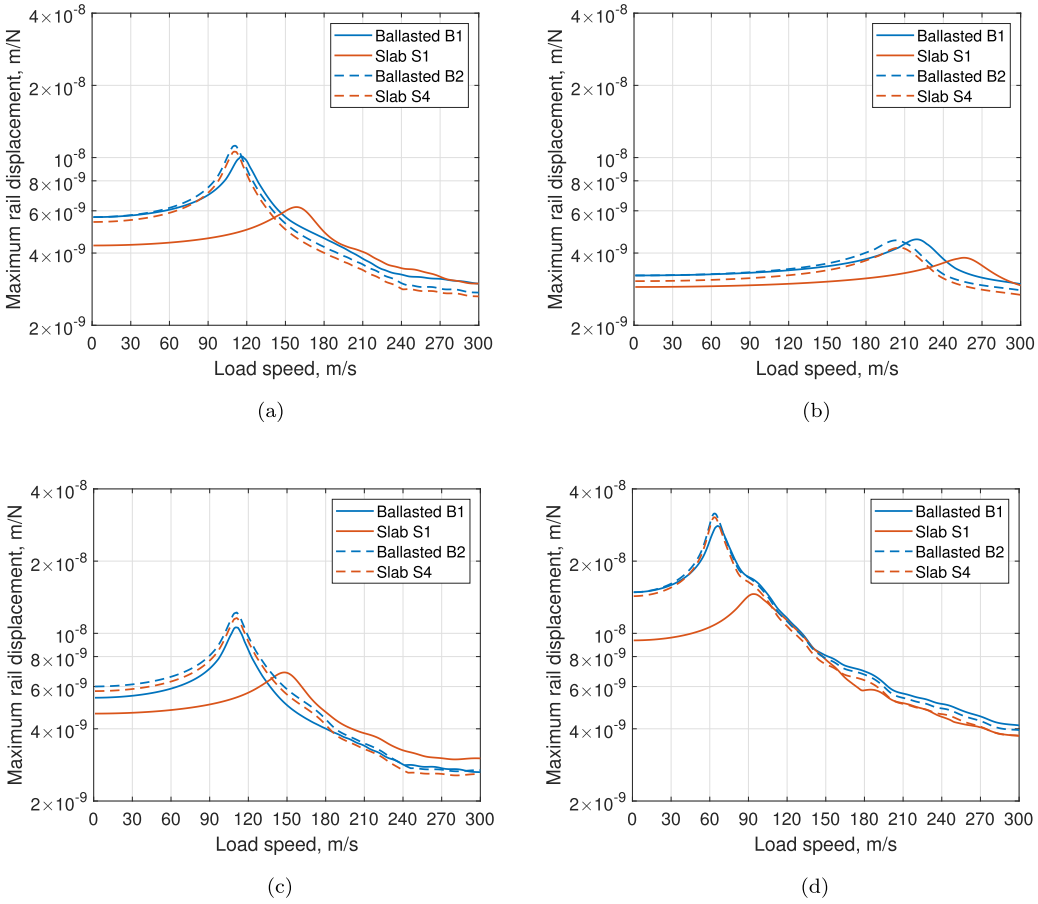

Fig. 22. Maximum rail displacement with load speed for ballasted track B1, slab track S1, ballasted track B2 and slab track S4 on: (a) ground Type G1; (b) ground Type G2; (c) ground Type G3; (d) ground Type G4.

Table 6
Values of the critical speed and dynamic amplification factor.

Ground	Track	Critical speed (m/s)	Dynamic amplification factor	Rayleigh wave speed of upper layer (m/s)
Type G1	Ballasted Case B1	115	1.79	109
	Slab Case S1	159 (+38%)	1.45	
Type G2	Ballasted Case B1	219	1.41	227
	Slab Case S1	256 (+17%)	1.32	
Type G3	Ballasted Case B1	115	1.84	109
	Slab Case S1	148 (+29%)	1.48	
Type G4	Ballasted Case B1	66	1.89	54
	Slab Case S1	94 (+42%)	1.56	
Type G5	Ballasted Case B1	135	1.50	109
	Slab Case S1	224 (+66%)	1.63	
Type G6	Ballasted Case B1	109	1.95	109
	Slab Case S1	109 (+0%)	1.49	

For the homogeneous ground Type G6 the value of the critical speed for ballasted track B1 (in Fig. 23(a)) is similar to the value for slab track S1 (in Fig. 23(b)). This value is equal to the Rayleigh wave speed of the half-space, as given in Table 6. In a homogeneous ground the P-SV waves are non-dispersive and the critical speed is determined by the properties of the ground and is not affected by the track properties [4,13,36]. For ground Type G5, with a reduced thickness of the surface layer, the critical speeds are higher than for ground Type G1 due to the increased influence of the underlying stiff half-space.

Results are also shown in Fig. 23(c) for slab track S5 which has reduced fastening stiffness. This has similar values of critical speed to slab track S1 although the track deflections are larger. Nevertheless the maximum deflection is still smaller for both the slab tracks than for the ballasted track; it is about 40% greater than the static deflection whereas for the ballasted track there is an increase of 100%. The static deflections are slightly smaller for the slab track with stiffness 120 MN/m than for the ballasted track, whereas with the reduced fastener stiffness they are slightly larger than for the ballasted track.

Conclusions

The differences in ground-borne vibration performance of typical ballasted and slab tracks have been assessed using a semi-analytical model. It is shown that there can be considerable differences between the vibration produced by different ballasted tracks, depending on the ground conditions and the ballast mass. Consequently, it is not straightforward to assign a ground vibration level difference between ballasted track and slab track as the result depends strongly on the reference case considered.

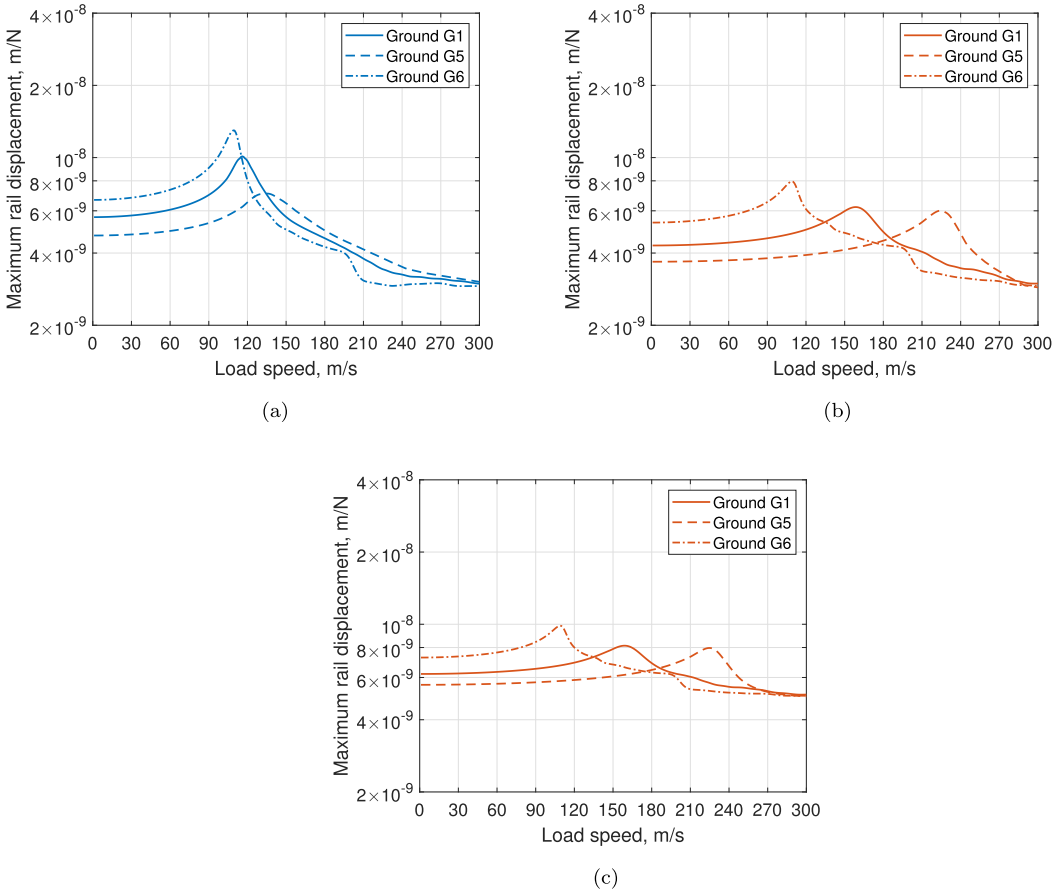

Fig. 23. Maximum rail displacement with load speed for ground Type G1, ground Type G5 and ground Type G6: (a) ballasted track B1; (b) slab track S1; (c) slab track S5.

The vibration performance of a ballasted track and a slab track have been shown to be very similar if an equivalent fastener stiffness is used. In the examples considered, the slab track produces 1–3 dB lower vibration for frequencies above about 16 Hz. This can be attributed to the slab mass rather than its bending stiffness. However, slab tracks are usually fitted with softer rail fasteners, in which case further substantial reductions occur above 63 Hz.

Measured loaded track unevenness levels for slab tracks can be considerably lower that those for typical ballasted tracks for wavelengths longer than 1 m. This results in substantianly lower ground vibration from slab tracks for frequencies that correspond to wavelengths longer than 1 m.

Examples of critical velocities on soft soils have also been evaluated. Here the bending stiffness of the slab offers some advantages; although there is little difference between the two track forms for a homogeneous soil, the slab track has higher critical velocities in the case of a layered soil with a softer upper layer and generally has lower maximum track deflections.

Acknowledgements

The work described here has been supported by the EPSRC under the programme grant EP/M025276/1, 'The science and analytical tools to design long life, low noise railway track systems (Track to the Future)' and the MOTIV project (Modelling of Train Induced Vibration), grants EP/K005847/2 and EP/K006002/1. All data published in this article are openly available from the University of Southampton repository at https://doi.org/10.5258/SOTON/D1001.

References

[1] Esveld C. Modern railway track. MRT Production, Zaltbommel (The Nederlands), 2nd ed.; 2001.
[2] Gautier P-E. Slab track: review of existing systems and optimization potentials including very high speed. Constr Build Mater 2015;92:9–15.
[3] Thompson DJ, Kouroussis G, Ntotsios E. Modelling, simulation and evaluation of ground vibration caused by rail vehicles. Veh Syst Dyn 2019;57(7):936–83.
[4] Sheng X, Jones CJC, Thompson DJ. A theoretical study on the influence of the track on train-induced ground vibration. J Sound Vib 2004;272(3–5):909–36.
[5] Steenbergen MJMM, Metrikine AV, Esveld C. Assessment of design parameters of a slab track railway system from a dynamic viewpoint. J Sound Vib 2007;306(1–2):361–71.
[6] Lombaert G, Degrande G, Vanhauwere B, Vandeborght B, François S. The control of ground-borne vibrations from railway traffic by means of continuous floating slabs. J Sound Vib 2006;297:946–61.
[7] Hussein MFM, Hunt HEM. Modeling of floating-slab tracks with continuous slabs under oscillating moving loads. J Sound Vib 2006;297:37–54.
[8] Hussein MFM, Hunt HEM. A numerical model for calculating vibration due to a harmonic moving load on a floating-slab track with discontinuous slabs in an underground railway tunnel. J Sound Vib 2009;321:361–71.
[9] Bian X, Jiang H, Chang C, Hu J, Chen Y. Track and ground vibrations generated by high-speed train running on ballastless railway with excitation of vertical track irregularities. Soil Dyn Earthq Eng 2015;76:29–43.
[10] Dai F, Thompson DJ, Zhu Y, Liu X. Vibration properties of slab track installed on a viaduct. Proc Inst Mech Eng, Part F: J Rail Rapid Transit 2016;230(1):235–52.
[11] Feng SJ, Zhang XL, Wang L, Zheng QT, Du FL, Wang ZL. In situ experimental study on high speed train induced ground vibrations with the ballast-less track. Soil Dyn Earthq Eng 2017;102:195–214.
[12] Thompson DJ. Railway noise and vibration: mechanisms, modelling and means of control. 1st ed. Oxford, UK: Elsevier; 2008.
[13] Costa PA, Colaço A, Calçada R, Cardoso AS. Critical speed of railway tracks. Detailed and simplified approaches. Transport Geotech 2015;2:30–46.
[14] Mezher SB, Connolly DP, Woodward PK, Laghrouche O, Pombo J, Costa PA. Railway critical velocity – analytical prediction and analysis. Transport Geotech 2016;6:84–96.
[15] Galvín P, Romero A, Domínguez J. Vibrations induced by HST passage on ballast and non-ballast tracks. Soil Dyn Earthq Eng 2010;30(9):862–73.
[16] Sheng X, Jones CJC, Thompson DJ. A theoretical model for ground vibration from

trains generated by vertical track irregularities. J Sound Vib 2004;272(3–5):937–65.
[17] Forrest JA, Hunt HEM. Ground vibration generated by trains in underground tunnels. J Sound Vib 2006;294(4):706–36.
[18] Forrest JA, Hunt HEM. A three-dimensional tunnel model for calculation of train-induced ground vibration. J Sound Vib 2006;294(4):678–705.
[19] Faure B, Bongini E. Results of the parameter studies and prioritization for prototype construction for ballasted track. RIVAS project. SCP0-GA-2010-265754 Report to the EC [Deliverable D3.2 – last accessed 30/03/2019]. <http://www.rivas-project.eu/fileadmin/documents/RIVAS_WP3_Del_3.2.pdf>.
[20] Rheda. Ballastless Track System brochure, Rail. One; 2000 [last accessed 30/03/2019]. <http://www.railone.com/fileadmin/daten/05-presse-medien/downloads/broschueren/en/Rheda2000_EN_2011_ebook.pdf>.
[21] MOTIV Homepage [last accessed 30/03/2019]. <https://motivproject.co.uk/>.
[22] Ntotsios E, Thompson D, Hussein M. The effect of track load correlation on ground-borne vibration from railways. J Sound Vib 2017;402:142–63.
[23] Hussein MFM, François S, Schevenels M, Hunt HEM, Talbot JP, Degrande G. The fictitious force method for efficient calculation of vibration from a tunnel embedded in a multi-layered half-space. J Sound Vib 2014;333(25):6996–7018.
[24] Sheng X, Jones CJC, Petyt M. Ground vibration generated by a load moving along a railway track. J Sound Vib 1999;228(1):129–56.
[25] Mirza A, Frid A, Nielsen JCO, Jones CJC. Ground vibration induced by railway traffic – the influence of vehicle parameters. In: Proceedings of the 10th international workshop on railway noise. Notes on numerical fluid mechanics and multidisciplinary design, vol. 118; 2012. p. 259–66.
[26] Triepaischajonsak N, Thompson DJ, Jones CJC, Ryue J, Priest JA. Ground vibration from trains: experimental parameter characterization and validation of a numerical model. Proc Inst Mech Eng, Part F: J Rail Rapid Transit 2011;225(2):140–53.
[27] Grassie SL, Saxon MJ, Smith JD. Measurement of longitudinal rail irregularities and criteria for acceptable grinding. J Sound Vib 1999;227(5):949–64.
[28] Verachtert R, Hunt HEM, Hussein MFM, Degrande G. Changes of perceived unevenness caused by in-track vibration countermeasures in slab track. Euro J Mech, A/Solids 65.
[29] Bastin R. Development of German non-ballasted track forms. Proc Inst Civil Eng: Transport 2006;159(1):25–39.
[30] Triepaischajonsak N, Thompson DJ. A hybrid modelling approach for predicting ground vibration from trains. J Sound Vib 2015;335:147–73.
[31] Kausel E, Roësset JM. Stiffness matrices for layered soils. Bull Seismol Soc Am 1981;35(6):1743–61.
[32] Sheng X, Jones CJC, Petyt M. Ground vibration generated by a harmonic load acting on a railway track. J Sound Vib 1999;225(1):3–28.
[33] Achenbach JD. Wave propagation in elastic solids. North-Holland series in applied mathematics and mechanics vol. 16. Amsterdam, The Netherlands: North-Holland; 1973.
[34] Kausel E. Fundamental solutions in elastodynamics: a compendium. New York: Cambridge University Press; 2006.
[35] Schevenels M, Francçois S, Degrande G. EDT: an elastodynamics toolbox for MATLAB. Comput Geosci 2009;35(8):1752–4.
[36] Dieterman HA, Metrikine A. Equivalent stiffness of a half-space interacting with a beam. Critical velocities of a moving load along the beam. Euro J Mech, A/Solids 1996;15(1):67–90.